



DOI: 10.21625/essd.v7i2.849

Geospatial Data Acquisition Using Unmanned Aerial Systems (Uas); A Paradigm for Mapping the Built Environment of the Niger Delta Region of Nigeria

LEONARD M.O AMINIGBO¹, JOSHUA BROWN², PRECIOUS N. EDE³*COASTAL RESEARCH GROUP (COREG)**Department of Geography and Environmental Management, Rivers state University, Portharcourt Nigeria.**P. M. B. 5080, Nkpolu-Oroworukwo, Rivers State, Nigeria**Email:leonard.aminigbo@ust.edu.ng, Joshua.brown@ust.edu.ng, precious.ede@ust.edu.ng**Phone numbers: 08030899971, 08033126784, 08062964674*

Abstract

The Rivers State University campus in Portharcourt is one of the university campuses in the city of Portharcourt, Nigeria covering over 21 square kilometers and housing a variety of academic, residential, administrative and other support buildings. The University Campus has seen significant transformation in recent years, including the rehabilitation of old facilities, the construction of new academic facilities and the most recent update on the creation of new collages, faculties and departments. The current view of the transformations done within the University Campus is missing from several available maps of the university. Numerous facilities have been constructed on the University Campus that are not represented on these maps as well as the qualities associated with these facilities. Existing information on the various landscapes on the map is outdated and it needs to be streamlined in light of recent changes to the University's facilities and departments. This research article aims to demonstrate the effectiveness of unmanned aerial systems (UAS) in geospatial data collection for physical planning and mapping of infrastructures at the Rivers State University Port Harcourt campus by developing a UAS-based digital map and tour guide for RSU's main campus covering all collages, faculties and departments and this offers visitors, staff and students with location and attribute information within the campus.

Methodologically, Unmanned Aerial Vehicles were deployed to obtain current visible images of the campus following the growth and increasing infrastructural development. At a flying height of 76.2m (250 ft), a DJI Phantom 4 Pro UAS equipped with a 20-megapixel visible camera was flown around the campus, generating imagery with 1.69cm spatial resolution per pixel. To obtain 3D modeling capabilities, visible imagery was acquired using the flight-planning software DroneDeploy with a near nadir angle and 75 percent front and side overlap.

Vertical positions were linked to the World Geodetic System 1984 and horizontal positions to the 1984 World Geodetic Datum universal transverse Mercator (UTM) (WGS 84). To match the UAS data, GCPs were transformed to UTM zone 32 north.

Finally, dense point clouds, DSM, and an orthomosaic which is a geometrically corrected aerial image that provides an accurate representation of an area and can be used to determine true distances, were among the UAS-derived deliverables.

© 2022 The Authors. Published by IEREK press. This is an open access article under the CC BY license (<https://creativecommons.org/licenses/by/4.0/>). Peer-review under responsibility of ESSD’s International Scientific Committee of Reviewers.

Keywords

UAS, Geospatial, Acquisition, Orthophoto, Mosaic, Flying –Height.

1. INTRODUCTION

Remote sensing is a technique for gathering data about items or the environment without having to come into direct contact with them. The electromagnetic energy (EME) reflected and/or emitted by such items is the primary medium of interaction. The radiant energy's intensity/brightness readings are gathered by a sensor, which is then calibrated and recorded as digital recordings of point-wise data. While the spatial groupings of intensities contain very specific geometric information about an object, the magnitudes of the intensities portray specific thematic or attribute information about the object.

Thus, it is feasible to infer the features of such objects both in terms of geometric (physical dimensions) and attribute characteristics by analyzing the patterns generated by the spatial distribution of intensities and variations in the magnitudes of the intensities of such recorded radiation (nature). Remote sensing is a technique for gathering information from a distance. The atmosphere reduces the contrast of all objects observed by aerial imaging in general. When two objects consisting of sand with a reflection coefficient of 30 and a coniferous forest with a reflection coefficient of 1, the object contrast, K can be stated as follows:

$$\frac{\rho_{\text{sand}}}{\rho_{\text{forest}}} = \frac{30}{1} = 30 = K \quad \dots\dots\dots \text{Eq. 1}$$

The visual contrast is then influenced by the 3 percent diffused ambient lights.

Thus:

$$K' = \frac{30+3}{1+3} = \frac{33}{4} = 8 = K' \quad \dots\dots\dots \text{Eq. 2}$$

This illustrates that resolutions of generally low-contrast aerial photographs should not be compared at a contrast of 1000:1, but at a contrast of 1.6:1, for which the modulation of 1 diminishes to 0.23. Thus, the modulation transfer function, as shown in Figure 2.38, is flattened, and its intersection with the limiting function of the eye is lowered in resolution.

Aerial survey camera systems with image motion compensation are, in practice, achieving a resolution of between 40 to 50 lp/mm for black-and-white images and of between 30 and 40 lp/mm for color images.

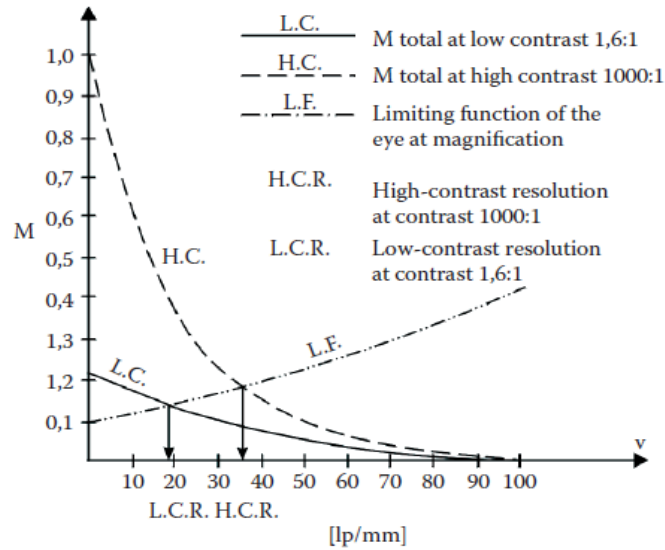
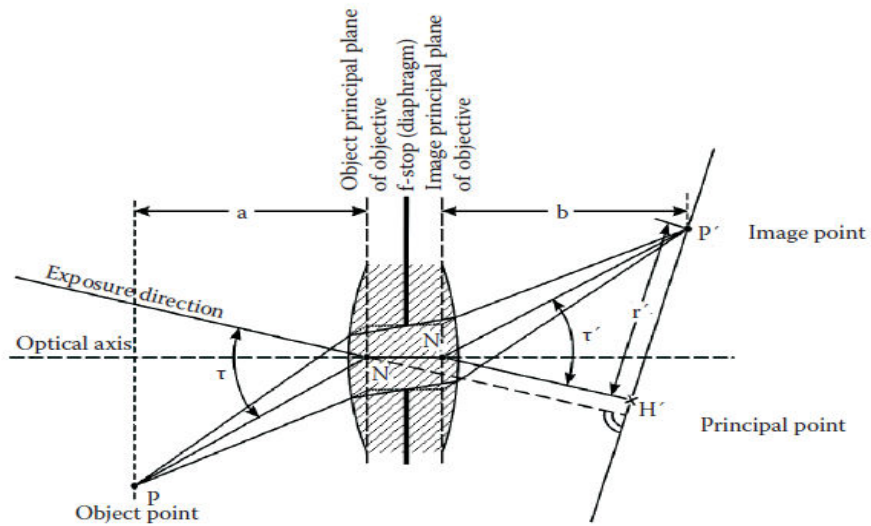


Fig. 1: Image resolution at low contrast



g. 2: Imaging through an objective.

Fi

1.1. Concepts for Image Mapping

Filtering

Each pixel's neighbouring pixels are used in filtering procedures. Local filters work with an image matrix, $D(x, y)$, that has a finite, usually small size, such as 3 3 or 5 5. A weight matrix, W , has been allocated to this matrix (x, y) . A convolution of the image matrix, $D(x, y)$, with the weight matrix, W , yields the outcome of the filtering process for each pixel, $d(x, y) (x, y)$.

Image (X, Y)

| | | |
|---------------|-------------|---------------|
| $d_{i-1,j-1}$ | $d_{i,j-1}$ | $d_{i+1,j-1}$ |
| $d_{i-1,j}$ | $d_{i,j}$ | $d_{i+1,j}$ |
| $d_{i-1,j+1}$ | $d_{i,j+1}$ | $d_{i+1,j+1}$ |

Image W (X, Y)

| | | | | | | | | |
|-----|-----|-----|------|------|------|------|---|------|
| 1/9 | 1/9 | 1/9 | +1/3 | +1/3 | +1/3 | +1/3 | 0 | -1/3 |
| 1/9 | 1/9 | 1/9 | 0 | 0 | 0 | +1/3 | 0 | -1/3 |
| 1/9 | 1/9 | 1/9 | -1/3 | -1/3 | -1/3 | +1/3 | 0 | -1/3 |

Low pass
Vertical direction
Horizontal direction

| | | | | | |
|----|----|----|----|----|----|
| 0 | +1 | +1 | +1 | +1 | 0 |
| -1 | 0 | +1 | +1 | 0 | -1 |
| -1 | -1 | 0 | 0 | -1 | -1 |

Diagonal direction
Diagonal direction

Figures 3 and 4 illustrate examples of a 3x3 image matrix, $D(x, y)$, and a number of key weight matrices, $W(x, y)$. From a practical standpoint, we can define image mapping as the science and art of capturing images of an object or environment and obtaining accurate geometric measurements from the images for various purposes such as the construction of planimetric and topographic maps (showing object surface details), classification of soils (object body makeup), interpretation of geology, military intelligence acquisition, and so on (mosaic). Image acquisition and image metrology are the two procedures that make up this system. Image acquisition is the process of planning and photographing the target object to be mapped, whereas image metrology is the art and science of recovering precise geometric measurements (size and shape) of the photographed object for positioning, mapping, navigation, and applications. We describe image mapping in this monograph as the dual processes of image production and object reconstruction from images. The image generation technique turns the three dimensions of the frequently enormous object space into a convenient two-dimensional image space, sacrificing one dimension of space in the process. On the other hand, image metrology (object reconstruction) aims to recover the original image, Skow, et al, (2017).

The image generation technique turns the three dimensions of the frequently enormous object space into a convenient two-dimensional image space, sacrificing one dimension of space in the process. On the other hand, image metrology (object reconstruction) aims to recover the three dimensions of the object space from the two dimensions of the picture space, which necessitates the discovery of the missing dimension. This sets the setting for a major engineering challenge in attempting to map the physical environment using a remote sensing instrument. This problem will be referred to as an image mapping problem in this book. We'll also recognize the technique of capturing an image of a target item (commonly referred to as imaging or photography).

The process of object reconstruction is known as the inverse problem of image mapping, while the direct problem of image mapping is known as image coverage.

In some real-world picture mapping applications, problems are frequently simplified by assuming that the target object or environment is flat and two-dimensional. Carlson, et al, (1997). This assumption is impractical and it considerably simplifies the problem to that of data transformation between two planes. This simplification is useful in situations where the target object's or environment's height isn't a concern. In general, a variety of techniques and methods have been used to solve the mapping problem.

One popular assumption is to treat the image's flat 2D space as a virtual 3D space, transforming the problem into a virtual 3D to 3D translation. Another new feature is the use of many images to cover the same target object or area Du, et al (2017). This opens up a lot of possibilities for solving the inverse problem we're dealing with. For example, the object can now be reconstructed using either a direct mathematical calculation or an indirect route of relative and absolute orientation, which can be done in a wholly mathematical or partially analogue and partly mathematical manner. It is also possible to extend the basic projector model to account for nuisance variables and perform an integrated object reconstruction with additional but different data types in what is known as SPAGIO.

The image mapping procedure can also be used as part of a set of sensors for dynamic applications like navigation and real-time position monitoring. The options are truly limitless.

The photographs are captured from space, from the air, or from a ground station. We're talking about photographs collected using a camera placed on a plane flying over the area or sensors on a satellite platform in this note. This is to make the presentation and understanding of the universal and adaptable principles and formulations for all mapping contexts easier. The optimum mapping approach for huge projects has yet to be developed: mapping using aerial pictures in addition, satellite-based image mapping is becoming increasingly common, particularly for planimetric features, maps and revisions on a small to medium size. The civilian and military mapping agencies of government are the primary consumers of aerial mapping methods. The essential characteristics and algorithms for gathering data for map construction from photos are thus; the film-based or digital cameras or sensors mounted on aircrafts pointing vertically downward, understanding the process of image generation and developing the mathematical relationship between points on the picture and points in the object space are both required for image metrology, picture formation is conceptualized as an optical projection of the item onto the image plane, the imaging ray, projector, optical bundle, or simply ray is the optical ray that enables this projection, perspective assures that all infinitely many rays from the object space travel via the same point on their way to the picture space, the projection center, perspective center, or exposure point are all names for the same place.

This notion is utilized to create projective equations for single camera to object space imaging as well as two or more cameras to object space imaging in the next sections. We should mention that in the multi-camera instance, two or more cameras cover the same region of the object space (i.e, overlapping images). The derivations are purely dependent on the theory of analytical vector geometry for ray tracing or modeling, whose basic equation is the straight line equation, which has been thoroughly explored in earlier chapters. We simply state that the equations used to solve the inverse problem of image mapping are the inverses of the equations used to solve the direct problem of mapping.

2. MATERIALS/METHODS

2.1. Data Gathering

Following the expansion and increased infrastructural development at portharcourt campus of Rivers state university, UAS surveys were conducted to obtain current visible imagery of the study area.

The study area was subdivided into four major quadrants A, B, C, D and E from a base map as shown in figure 1.

UAS surveys were done to obtain current visible images of the campus following the growth and increasing infrastructural development at Rivers state university's portharcourt campus.

At a flying height of 76.2m (250 ft), a DJI Phantom 4 Pro UAS equipped with a 20-megapixel visible camera was flown around the campus, generating imagery with 1.69cm spatial resolution per pixel. To obtain 3D modeling capabilities, visible imagery was acquired using the flight-planning software DroneDeploy with a near nadir angle and 75 percent front and side overlap (Westoby et al. 2012;). Over 2000 photo images of the study area were acquired on the 18 May 2020 in mostly cloud-free sky and excellent light circumstances (low zenith angle) to reduce cloud shadows. Ground control surveys were carried out to guarantee the data's geographic accuracy. Trimble Geo7x ground control survey equipment with global navigation was used to collect ground control points (GCPs).

With a precision of 60.4 cm, this device permitted high-accuracy ground surveying and precise point measuring. The 10 points (GCPs) were gathered using 1m-31m targets placed around the study area and at various elevation levels. Vertical positions were linked to the World Geodetic System 1984 and horizontal positions to the 1984 World Geodetic Datum universal transverse Mercator (UTM) (WGS 84). To match the UAS data, GCPs were transformed to UTM zone 32 north (UTM 32N).

The data gathered was transferred from the UAS storage devices to a laptop, which was running on a generator. It was an immense effort, resulting in an unprecedented amount of information (almost 10,000 photos totaling 50GB) with a resolution of roughly a square inch per pixel. All images were processed into a single Pix4Dmapper file in just under 46 hours, producing a 3D densified point cloud, a 3D textured mesh and a high-resolution 15GB orthomosaic map.



Figure 1: Ortho-Photo Base Map of Rivers state University Portharcourt campus.

2.2. Data Preparation

Agisoft Metashape Professional (Agisoft 2019) was used to process UAS footage and create post-event imagery and 3D-modeling solutions (DSM and point cloud). To reduce positional distortions of 1–10 cm caused by camera GPS location inaccuracies, UAS pictures were co-registered to GCPs (Johnson et al, 2018).

Due to changes in lighting conditions, color corrections were made using the calibrate color technique in Agisoft Metashape Professional to equalize brightness values over the entire dataset. Dense point clouds, DSM, and an orthomosaic, a geometrically corrected aerial image that provides an accurate representation of an area and can be used to determine true distances, were among the UAS-derived deliverables.

3. RESULTS AND ANALYSES

In zone A the open space beside Geology department opposite Law faculty is the largest vacant space with a total area of 2,543.20 sqm while in zone B the largest vacant space of 62,143.86 sqm is located at the back of the department of forestry and research farm.

Environmental Science and Sustainable Development

In zone C, Open space adjoining the main gate opposite the Catholic Church is the largest vacant space within the zone with a total area of 32,666.07 sqm while in zone D, Open space in front of S.U.G secretariat and love garden is the largest vacant space with a total area of 6,543.87sqm.

In zone E, Open space along the amphitheatre/old faculty of management science and back of faculty of engineering is the largest vacant space within the zone with a total area of 6,453.65sqm.

Finally, the largest vacant space of 62,143.86 sqm is located at the back of the department of forestry and research farm which is in zone B.

Using Pix4Dmapper, a number of outputs including topographic maps were used to plot carefully the built portions of Rivers state university porttharcourt campus.

The drone survey was also used to create a ‘fly-through’ video which was presented to the university management.

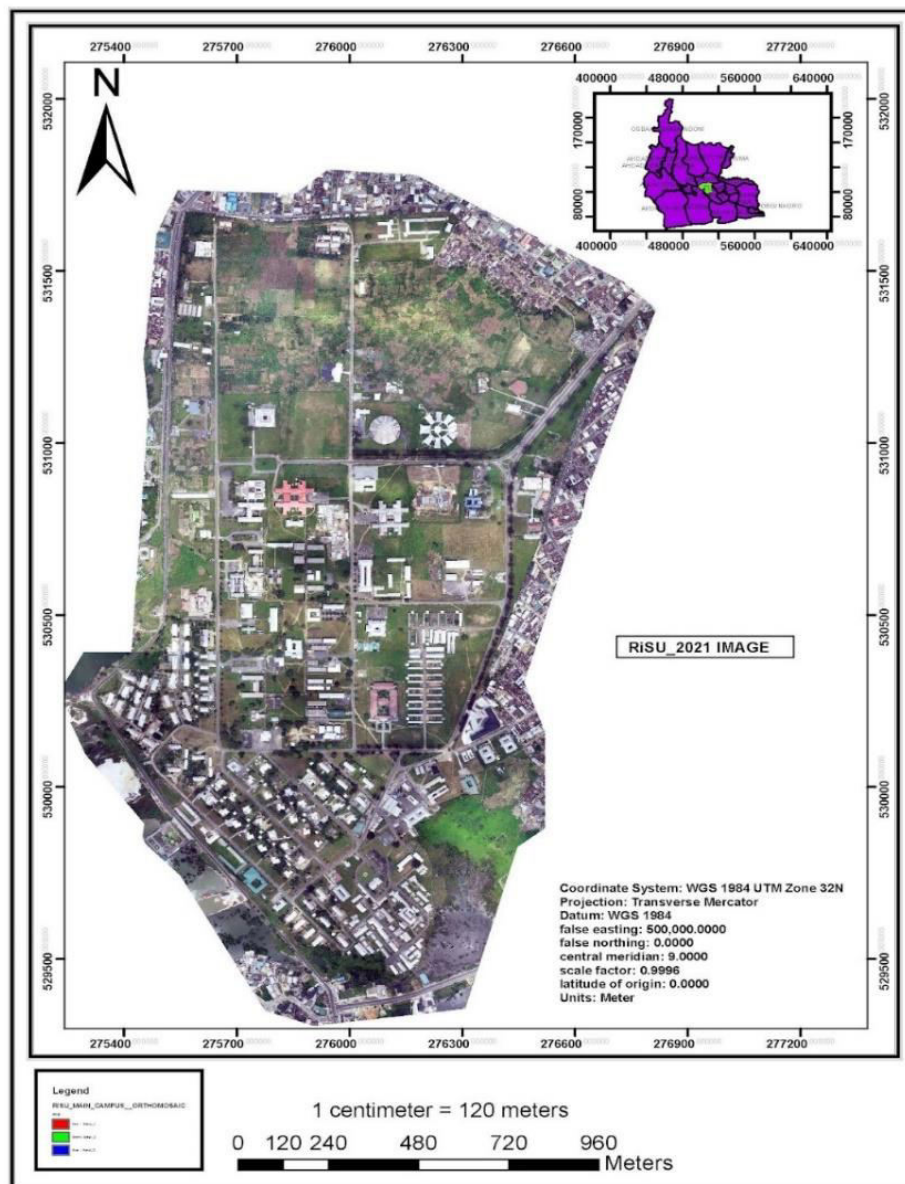


Figure 1: 2021 UAS Acquired Imagery of Rivers State University Portharcourt campus.

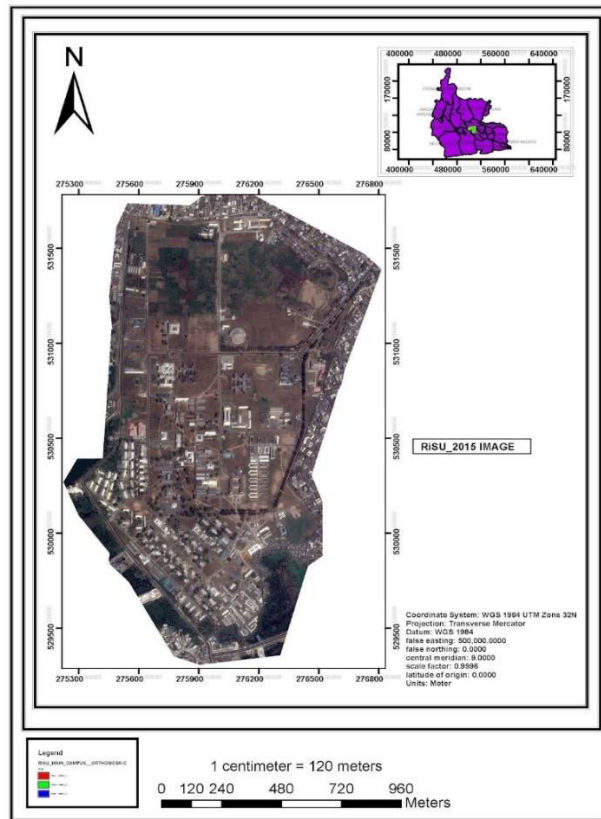


Figure 2: 2015 Sentinel Imagery of Rivers State University Portharcourt campus.

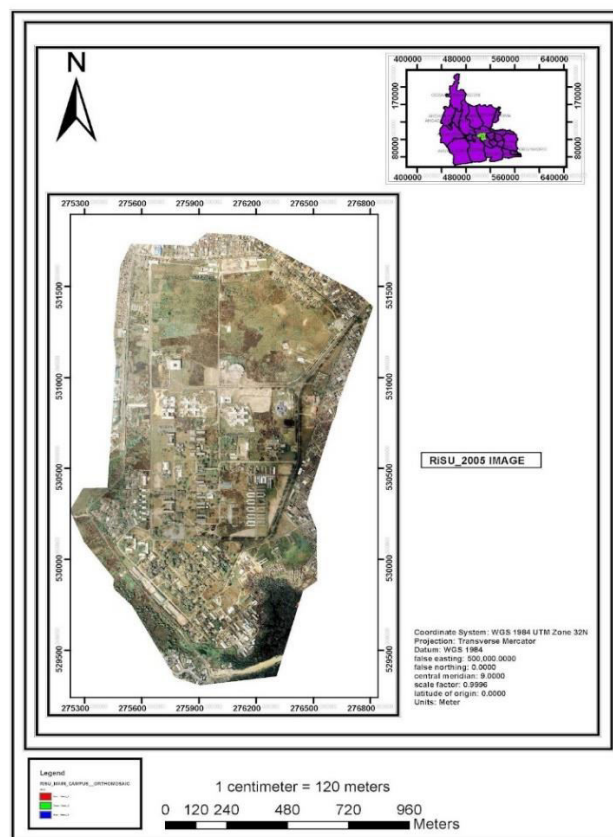


Figure 3: 2005 Orthophoto Imagery of Rivers State University Portharcourt campus.

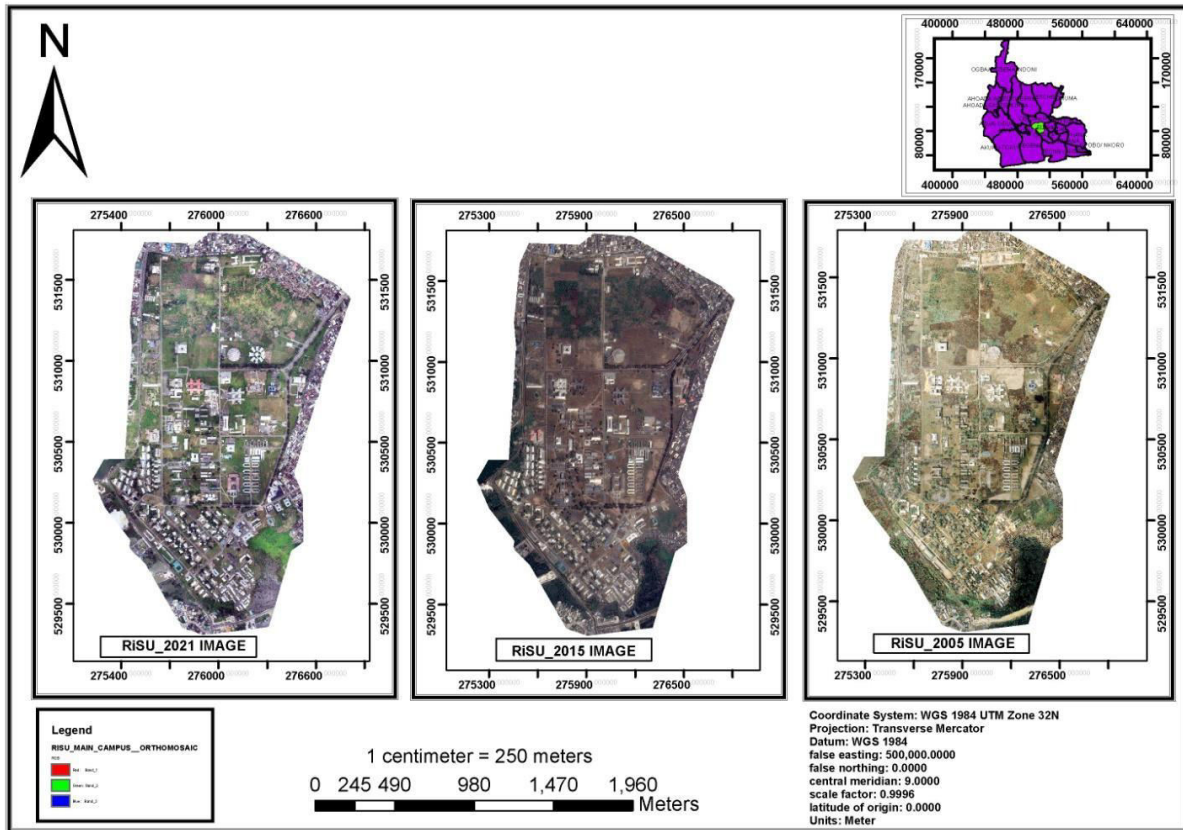


Figure 4: Composite Imageries of Rivers State University Portharcourt campus, 2021, 2015 and 2005.

Open Spaces in Zone (A)

Table 1: Location and sizes of Open Spaces in Zone (A)

| S/N | Open space Identification | COORDINATES | | | |
|-----|--|------------------|-------------------|--------------------|------------|
| | | EASTING (meters) | NORTHING (meters) | ELEVATION (meters) | AREA (sqm) |
| 1 | Open space beside Geology Department /opposite Law Faculty | 275617.308m | 530913.943m | 8.60 | 2543.20 |
| 2 | Open space between NEEDS Assessment and Medical Centre | 275585.950m | 530688.805m | 1.28 | 2276.45 |

Table 1: Location and sizes of Open Spaces in Zone (A)

In zone A, the open space beside Geology Department is the largest vacant space within the zone with a total area of 2, 543 sqm.

Open Space in Zone (B)

Table 2: Location and sizes of Open Spaces in Zone (B)

| S/N | Open space Identification | CORDINATES | | | |
|-----|---|---------------|---------------|---------------|---------------|
| | | E (meters) | N (meters) | Z (meters) | AREA (sqm) |
| 1 | Open space within the faculty of environmental sciences | 275929.347m | 530906.575m | 10.55m | 2754.86 |
| 2 | Open space in between the central library and convocation arena | 275928.985m | 531033.854m | 12.47 | 44372.86 |
| 3 | Open space at the back of department of forestry, environment of teaching and research farm and central library | 275803.015m | 531364.656m | 13.25 | 62143.86 |
| 4 | Open space between information technology centre and engineering faculty | 275715.758m | 530424.619m | 6.50m | 2875.86 |

Table 2: Location and sizes of Open Spaces in Zone (B)

In zone B, the open space Open space at the back of the department of forestry and research farm is the largest vacant space within the zone with a total area of 62,143.86 sqm.

Open Space in Zone (C)

Table 3: Location and sizes of Open Spaces in Zone (C)

| S/N | Open space Identification | CORDINATES | | | |
|-----|---|---------------|---------------|---------------|---------------|
| | | E (meters) | N (meters) | Z (meters) | AREA (sqm) |
| 1 | Open space behind management sciences | 276128.555m | 530694.479m | 14.56 | 9822.7 |
| 2 | Farm land between security village and convocation arena | 276215.134m | 531365.487m | 10.22 | 135447.48 |
| 3 | Open space adjoining the main gate opposite the Catholic Church | 276599.231m | 531118.142m | 12.63 | 32666.07 |
| 4 | Open space of Maracana stadium and NDDC female hostel | 276152.679m | 530153.019m | 11.33m | 16782.54 |

Table 3: Location and sizes of Open Spaces in Zone (C)

In zone C, Open space adjoining the main gate opposite the Catholic Church is the largest vacant space within the zone with a total area of 32,666.07 sqm.

Open Space in Zone (D)

Table 4: Location and sizes of Open Spaces in Zone (D)

| S/N | Open space Identification | CORDINATES | | | |
|-----|--|--------------|-------------|------------|------------|
| | | E (meters) | N (meters) | Z (meters) | AREA (sqm) |
| 1 | Open space behind Catholic Church, motor park and security village | 276411.385m | 531266.225m | 17.42 | 184600.71 |
| 2 | Open space in between the senate building and works department | 276342.996m | 530729.560m | 13.51 | 15618.7 |
| 3 | Open space behind F and G/H hostels | 2766319.618m | 530374.609m | 15.66 | 7286.78 |
| 4 | Open space adjacent to the filling station | 276453.816m | 530639.481m | 16.10 | 11940.59 |
| 5 | Open space behind the college of medicine and NDDC female hostel | 276084.516m | 530350.933m | 12.35 | 5377.49 |
| 6 | Open space adjoining back gate behind the F.C.B.B P/G hostel | 276435.493m | 530019.948m | 8.52 | 4426.97 |
| 7 | Open space in front of hostel E and basket ball court | 2756104.142m | 529808.830m | 9.21 | 2384.93 |
| 8 | Open space along road (C) opposite old V.C complex | 275968.679m | 529819.988m | 7.44 | 28635.05 |
| 9 | Open space directly opposite the U.B.A/Polaris bank | 276060.182m | 530072.917m | 9.89 | 6048.76 |
| 10 | Open space in front of S.U.G secretariat and love garden | 276180.704m | 530084.099m | 10.48 | 6543.87 |

Table 4: Location and sizes of Open Spaces in Zone (D)

In zone D, Open space in front of S.U.G secretariat and love garden is the largest vacant space within the zone with a total area of 6543.87sqm.

Open Space in Zone (E)

Table 5: Location and sizes of Open Spaces in Zone (E)

| S/N | Open space Identification | CORDINATES | | | |
|-----|--|-------------|-------------|-------|------------|
| | | E | N | Z | AREA (sqm) |
| 1 | Open space along road A and road B junction adjoining the lecturers quarters | 275612.237m | 530126.427m | 9.33 | 12648.79 |
| 2 | Open space along the amphitheatre/old faculty of management science and back of faculty of engineering | 275679.174m | 530245.010m | 12.70 | 6453.65 |

In zone E, Open space along the amphitheatre/old faculty of management science and back of faculty of engineering is the largest vacant space within the zone with a total area of 6453.65sqm.

4. CONCLUSION

From the image data obtained from DJI UAS, Pix4Dmapper application was used to generate a 3D point cloud and 2D orthomosaic of the campus in high resolution. The on-site flight and ground survey took one day, and processing this data required an additional two days.

Combined with data gathered on the ground with handheld GPS units, the university now has a comprehensive map of built and vacant areas that will be used to plan and manage infrastructure assets within the campus.

This lofty ambition is built on the basemap created with UAS. “The basemap becomes a two-way source of conversation, connection and interactions within the university community and the general visiting public and the results of this project will have undoubtedly impact on policy making by university authorities.

The output of this study will act as a baseline that can be compared to future images to monitor potential changes over time and will be of vital importance in physical infrastructural planning and management within the university campus.

Finally, dense point clouds, DSM, and an orthomosaic which is a geometrically corrected aerial image that provides an accurate representation of an area and can be used to determine absolute and relative locations of places and features on campus. True distances and bearings between two points can also be computed from the UAS-derived orthophoto mosaic dataset.

REFERENCES

- Agisoft, 2019: Agisoft Metashape user manual: Professional edition version 1.5. AgisoftLLC Doc., 145pp., https://www.agisoft.com/pdf/metashape-pro_1_5_en.pdf.
- Ahmed, N. S., 2016: Field observations and computer modeling of tornado-terrain interaction and its effects on tornado damage and path. Ph.D. dissertation, The University of Arkansas, 247 pp., <http://scholarworks.uark.edu/etd/1463>.
- Bosart, L. F., A. Seimon, K. D. LaPenta, and M. J. Dickinson, 2006: Supercell tornadogenesis over complex terrain: The Great Barrington, Massachusetts, tornado on 29 May 1995. *Wea. Forecasting*, 21, 897–922, <https://doi.org/10.1175/WAF957.1>.
- Carlson, T. N., and D. A. Ripley, 1997: On the relation between NDVI, fractional vegetation cover, and leaf area index. *Remote Sens. Environ.*, 62, 241–252, [https://doi.org/10.1016/S0034-4257\(97\)00104-1](https://doi.org/10.1016/S0034-4257(97)00104-1).
- Carrivick, J. L., M. W. Smith, and D. J. Quincey, 2016: *Structure from Motion in the Geosciences*. John Wiley and Sons, 197 pp.
- Chen, Q. J., Y. R. He, T. T. He, and W. J. Fu, 2020: The typhoon disaster analysis emergency response system based on UAV 2832 MONTHLY WEATHER REVIEW VOLUME 149 remote sensing technology. *Int. Arch. Photogramm. Remote Sens. Spat. Info. Sci.*, XLII-3/W10, 959–965, <https://doi.org/10.5194/isprs-archives-XLII-3-W10-959-2020>.
- Coleman, T. A., 2010: The effects of topography and friction on mesocyclones and tornadoes. 25th Conf. on Severe Local Storms, Denver, CO, Amer. Meteor. Soc, P8.12, <https://ams.confex.com/ams/25SLS/techprogram/paper176240.htm>.
- DiCiccio, T. J., and J. P. Romano, 1990: Nonparametric confidence limits by resampling methods and least favorable families. *Int. Stat. Rev.*, 58, 59–76, <https://doi.org/10.2307/1403474>.
- Du, M., and N. Noguchi, 2017: Monitoring of wheat growth status and mapping of wheat yield’s within-field spatial variations using color images acquired from UAV-camera system. *Remote Sens.*, 9, 289, <https://doi.org/10.3390/rs9030289>.
- Efron, B., 1981: Nonparametric standard errors and confidence intervals. *Can. J. Stat.*, 9, 139–158, <https://doi.org/10.2307/3314608>, and
- Ezequiel, C. A. F., and Coauthors, 2014: UAV aerial imaging applications for post-disaster assessment, environmental management and infrastructure development. *Int. Conf. on Unmanned Aircraft Systems*, Orlando, FL, IEEE, 274–283.
- Heredia, G., F. Caballero, I. Maza, L. Merino, A. Viguria, and A. Ollero, 2009: Multi-unmanned aerial vehicle (UAV) cooperative fault detection employing differential global positioning (DGPS), inertial and vision sensors. *Sensors*, 9, 7566–7579.
- Hesterberg, T. C., 1999: Bootstrap tilting confidence intervals and hypothesis tests. *Comput. Sci. Stat.*, 31, 389–393.
- Lyza, A. W., and K. R. Knupp, 2014: An observational analysis of potential terrain influences on tornado behavior. 27th Conf. on Severe Local Storms, Madison, WI, Amer. Meteor. Soc., 11A.1A, <https://ams.confex.com/ams/27SLS/webprogram/Paper255844.html>.
- Smith, M. S., 2006: Exploring local “tornado alleys” for predictive environmental parameters. *Proc. 2006 ESRI Int. User Conf.*, ESRI, 28 pp., https://proceedings.esri.com/library/userconf/proc06/papers/papers/pap_1339.
- Skow, K. D., and C. Cogil, 2017: High-Resolution aerial survey and radar analysis of quasi-linear convective system surface vortex damage paths from 31 August 2014. *Wea. Forecasting*, 32, 441–467, <https://doi.org/10.1175/WAF-D-16-0136.1>.
- Tmu_sic, G., and Coauthors, 2020: Current practices in UAS-based environmental monitoring. *Remote Sens.*, 12, 1001, <https://doi.org/10.3390/rs12061001>.

Environmental Science and Sustainable Development

- Wagner, M., and R. K. Doe, 2017: Using Unmanned Aerial Vehicles (UAVs) to model tornado impacts. 2017 Fall Meeting, San Francisco, CA, Amer. Geophys. Union, Abstract NH31A-0198.
- Johnson, Z. Chen, J. Das, and R. S. Cerveny, 2019: Unpiloted aerial systems (UASs) application for tornado damage surveys: Benefits and procedures. *Bull. Amer. Meteor. Soc.*, 100, 2405–2409, <https://doi.org/10.1175/BAMS-D-19-0124.1>.
- Wang, X., M. Wang, S. Wang, and Y. Wu, 2015: Extraction of vegetation information from visible unmanned aerial vehicle images. *Nongye Gongcheng Xuebao*, 31, 152–159, <https://doi.org/10.3969/j.issn.1002-6819.2015.05.022>.